Article type : MS - Regular Manuscript

In vivo phospho*enol*pyruvate carboxylase activity is controlled by CO_2 and O_2 mole fraction and represents a major flux at high photorespiration rates

Cyril Abadie and Guillaume Tcherkez*

Research School of Biology, Australian National University, 2601 Canberra ACT, Australia

*Corresponding author: guillaume.tcherkez@anu.edu.au; Tel. +61 (0)2 6125 0381.

Received: *11 September 2018*
Accepted: *23 September 2018*

ORCID

Guillaume Tcherkez https://orcid.org/0000-0002-3339-956X

Summary

• Phosph*enol*pyruvate carboxylase (PEPC)-catalyzed fixation of bicarbonate to C_4-acids is commonly believed to represent a rather small flux in illuminated leaves. In addition, its potential variation with O_2 and CO_2 is not documented and thus usually neglected in gas-exchange studies.

• Here, we used quantitative NMR analysis of sunflower leaves labelled with $^{13}CO_2$ (99% ^{13}C) under controlled conditions and measured the amount of ^{13}C found in the four C-atom positions in malate, the major product of PEPC activity.

• We found that amongst malate ^{13}C-isotopomers present after labelling, most molecules were labelled at both C-1 and C-4, showing the incorporation of ^{13}C at C-4 by PEPC fixation and subsequent redistribution to C-1 by fumarase (malate-fumarate equilibrium). In addition, absolute quantitation of ^{13}C-content showed that PEPC fixation increased at low CO_2 or high O_2, and represented up to 1.8 µmol m^{-2} s^{-1}, that is, 40% of net assimilation measured by gas exchange under high O_2/CO_2 conditions.

• Our results show that PEPC fixation represents a quantitatively important CO_2-fixing activity that varies with O_2 and/or CO_2 mole fraction and this challenges the common interpretation of net assimilation in C_3 plants, where PEPC activity is often disregarded or supposed to be constant at a very low rate.

Keywords: PEPC, photosynthesis, photorespiration, flux, CO_2

Introduction

Anaplerotic carbon fixation in C_3 plants involves phospho*enol*pyruvate carboxylase (PEPC, EC 4.1.1.31), which combines bicarbonate (HCO_3^-) with phospho*enol*pyruvate, thereby producing oxaloacetate (OAA) in the cytoplasm [and also in the chloroplast in rice (*Oryza sativa*), where a chloroplastic isoform has indeed been found (Masumoto *et al.*, 2010)]. After ribulose 1,5-bisphosphate carboxylase/oxygenase (Rubisco), PEPC is believed to the most significant carboxylase (Chollet *et al.*, 1996). In fact, in C_3 species, PEPC activity is essential to generate OAA that participates in malate-OAA shuttles between cellular compartments, replenishes the tricarboxylic acid pathway (TCAP) or simply leads to malate accumulation. In the illuminated leaf, PEPC activity appears to be disconnected from the TCAP since OAA is mostly reduced to malate (which can in turn be converted to fumarate) rather than consumed by citrate synthase (Fig. 1) (Tcherkez *et al.*, 2009). It has indeed been shown that nitrogen assimilation (to glutamate and glutamine) mostly remobilizes carbon skeletons that were produced previously during the night period (Gauthier *et al.*, 2010). Therefore, the metabolic role of PEPC activity in the light is mostly to synthesize OAA for aspartate (and amino acids derived therefrom, such as methionine) synthesis and modulate reductive power via reduction to malate. This phenomenon is believed to be at the origin of light enhanced dark respiration, whereby the decarboxylation of accumulated malate by the malic enzyme leads to an increased CO_2 release just after illumination, with naturally ^{13}C-enriched CO_2 (Gessler *et al.*, 2009). During the night, PEPC replenishes the TCAP to compensate for the synthesis and export of glutamine and asparagine to sink organs. The role of PEPC activity in sustaining nitrogen metabolism *in vivo* has been shown using isotopic methods and inhibitors in unicellular algae (Amory *et al.*, 1991; Turpin *et al.*, 1991). It is further supported by the metabolic phenotype of mutants affected in PEPC activation by PEPC kinase that have an altered content in several amino acids (Meimoun *et al.*, 2009).

Despite this importance in day and night gas exchange, the regulation of PEPC activity by photosynthetic conditions is not well-known. *In vitro*, C_3 PEPC activity has been shown to be inhibited by its product (malate) and glutamate, but stimulated by fructose 6-phosphate and glucose 6-phosphate (Krömer *et al.*, 1996b). *In vivo*, PEPC activity is controlled by PEPC kinase (PK): in its phosphorylated form, the enzyme is more active and less sensitive to allosteric inhibitors and more sensitive to allosteric activators [for a recent review, see (O'Leary & Plaxton, 2017)]. In most C_3 species, the enzyme has been found to be

dephosphorylated in the dark, and accordingly a lower PEPC activity has been measured on darkened leaf extracts compared to the light (Krömer *et al.*, 1996a) – although in some hygrophytic C_3 monocots, PEPC phosphorylation has been found to be higher at night (Fukayama *et al.*, 2006; Fukayama *et al.*, 2014). Phosphoproteomics conducted on illuminated Arabidopsis rosettes under controlled CO_2 and O_2 mole fraction have shown that there is a slight decrease in phosphorylation of isoform PEPC1 at high CO_2 (1000 µmol mol^{-1}) and low oxygen (0.03% O_2), suggesting that PEPC activity is down-regulated at high photosynthetic rates (Abadie *et al.*, 2016b). Our previous metabolomics analyses in sunflower leaves have shown that the malate content correlates with photorespiration, suggesting that malate biosynthesis is stimulated at low carboxylation and high oxygenation (data summarized in Fig S1) (Abadie *et al.*, 2016a). Also, detailed examination of ^{13}C-NMR signals in aspartate C-2 and C-3 atom positions have suggested an increase of PEPC activity at low CO_2 (Abadie *et al.*, 2017b).

However, there is currently no direct measurement of the *in vivo* PEPC flux under different photosynthetic conditions. This lack of knowledge is problematic to precisely understand CO_2 exchange in the illuminated leaf. In fact, PEPC activity may vary with CO_2 mole fraction. This effect might have to be taken into account when interpreting photosynthesic response to CO_2 (A/c_i curves). PEPC activity is commonly believed to be small or negligible, of a few percent of net assimilation and is therefore disregarded in C_3 photosynthetic models (von Caemmerer, 2013). Also, in natural carbon isotope balance, the potential impact of PEPC activity on net CO_2 exchange could be significant (Raven & Farquhar, 1990) because its ^{12}C/^{13}C isotope fractionation (about –5.2‰ with respect to dissolved CO_2) (O'Leary *et al.*, 1981; Marlier & O'Leary, 1984) is very different from that of Rubisco (29‰ in C_3 plants) (Roeske & O'Leary, 1984).

Here, we used NMR technology to provide a direct measurement of *in vivo* PEPC activity and answer the following questions: Is the rate if PEPC-catalyzed fixation negligible compared to net photosynthesis? Does it vary with the carboxylation-to-oxygenation ratio (i.e., with photorespiration)? To do so, we examined the labelling pattern in malate upon $^{13}CO_2$ labelling of sunflower leaves in the light, under five O_2/CO_2 conditions. When gaseous CO_2 is labelled (99% ^{13}C), leaf bicarbonate is also labelled and thus PEPC activity fixes ^{13}C-bicarbonate onto PEP. PEP itself can be labelled since it originates from triose phosphates which are photosynthetic products. To perform our PEPC activity measurements, we took advantage of two key features:

(i) the non-cyclicity of the TCAP, that leads to minimal loss of the ^{13}C-label from malate (we further show here the small utilization to fumarate and aspartate production, compared to malate) and minimal malate labelling via citrate and the right branch of the TCAP (Tcherkez *et al.*, 2009);

(ii) the fast equilibrium between CO_2 and HCO_3^- leading to complete ^{13}C-labelling in cellular bicarbonate very quickly. In fact, assuming cytoplasmic dissolved CO_2 is 9.5 µM (equivalent to 280 µmol mol^{-1} in gas phase) and cytoplasmic pH is 7.8, since 97.8% of dissolved inorganic carbon is in the form of bicarbonate at this pH, we have 9.5/0.022 = 432 µM bicarbonate in the cytoplasm. The CO_2 turn-over rate in the cytoplasm is given by the unidirectional flux equal to the product of internal conductance (gaseous, cell wall and plasma membrane components) and intercellular mole fraction ($g_{mw} \times c_i$) and thus is in the order of 0.1 mol m^{-2} s^{-1} × 280 µmol mol^{-1} = 28 µmol m^{-2} s^{-1}. That is, since 1 m² ≈ 260 g water in sunflower, a minimal concentration-based flux of 0.107 µmol mL^{-1} s^{-1} = 0.107 mM s^{-1} (in practice, this renewal rate is probably much larger because cytoplasm volume represents about 10% only of cellular volume and leaf water also comprises vein water, not only lamina water). Thus, the cytoplasmic pool of dissolved CO_2 is renewed within 9.5/107 = 0.09 s. Bicarbonate renewal depends on cytoplasmic carbonic anhydrases (CA) that are extremely efficient (nearly instantaneous equilibrium), and takes 432/107 = 4 s maximum. Thus, in principle bicarbonate should be labelled very quickly after having switched to $^{13}CO_2$. Equilibration experiments with air containing super high CO_2 mole fraction (up to 16% CO_2) have indeed shown that the first time constant for CO_2 equilibrium is 5 s (Oja *et al.*, 1999).

After ^{13}C-labelling, we performed NMR measurements and improved the NMR signal resolution of carboxylic groups using EDTA. We were able to measure the ^{13}C-enrichment in all C-atom positions of malate and calculated ^{13}C-fixation rates. Our results show that malate molecules were substantially labelled at C-1 and C-4 atom positions, showing *in vivo* PEPC activity. In addition, observed flux values show that PEPC-catalyzed fixation was neither small nor constant with different O_2/CO_2 environments.

Material and methods

Plant material

Sunflower seeds (*Helianthus annuus*, var. XRQ) were sown in potting mix and after 14 days, plantlets were transferred to 15 L pots. Plants were grown in the greenhouse under 24/18°C, 60/55% relative humidity, 16/8h photoperiod (day/night), with natural light supplemented by

Lucagrow 400 W sodium lamps (JB Lighting, Cheltenham, Australia). Plants were watered every two days supplemented once a week with 1.5 g L^{-1} nutrient solution Peters® Professional Pot Plant Special (Everris, the Netherlands) with a $N/P_2O_5/K_2O$ composition of 15/11/29 (and a nitrogen balance nitrate/ammonium/urea of 8.6/2.0/4.4) and trace elements.

Gas exchange and sampling

Gas-exchange under controlled O_2/CO_2 conditions was performed in a chamber coupled to the LI-COR 6400-XT (LI-COR Biosciences, USA) and having soft walls allowing instant sampling by liquid nitrogen spraying, as described previously (Tcherkez *et al.*, 2012). The leaf chamber was adapted to individual leaves with a surface area of about 100 cm². Light was supplied by a LED panel RGBW-L084 (Walz, Germany). Gas-exchange conditions were: 400 µmol m^{-2} s^{-1} photosynthetically active radiation (PAR), 80% relative humidity, gas flow 35 L h^{-1}, and 21-23°C air temperature. Isotopic labelling was performed using $^{13}CO_2$ (Sigma-Aldrich, 99% ^{13}C) for 2 h after having reached steady photosynthesis using ordinary CO_2 (natural abundance) for *ca*. 60 min. For all O_2/CO_2 conditions, two series of experiments were done: with $^{13}CO_2$, and with natural CO_2. Performing experiments with natural CO_2 was strictly required for $\%^{13}C$ calculations using NMR data. The five O_2/CO_2 conditions presented here are (%/µmol mol^{-1}, ordered by increasing carboxylation-to-oxygenation ratio): 100/380, 21/140, 21/380, 21/800, 2/380.

Extraction and NMR analysis

Samples were extracted with perchloric acid in liquid nitrogen as previously described in (Aubert *et al.*, 1994). Briefly, the sample was ground with 900 µL perchloric acid 70% and 500 µL maleic acid 0.5 M (i.e. a total of 125 µmol per sample, used as an internal standard). The powder was poured in a 50-mL centrifuge tube and then 10 mL MilliQ water were added. After centrifugation (15,000 ***g***, 15 min), the pellet was re-extracted with 3 mL perchloric acid 2% and centrifuged. The two supernatants were combined, the pH was adjusted to 5 with potassium hydroxide and the sample was frozen-dried. The sample was re-suspended in 1 mL MilliQ water and centrifuged, and the pH was adjusted to 7. 550 µL were transferred in a new tube, 50 µL D_2O were added and the sample was vortexed and poured in a 5-mm NMR tube (Z107373, Bruker Biospin). NMR analysis was then carried out (acquisition without EDTA). Just after analysis, the sample was transferred in an Eppendorf tube, frozen-dried, re-suspended in 600 µL EDTA 12.5 mM at pH 7.8, and 50 µL D_2O were added. After

centrifugation, 600 µL were collected and poured in a new NMR tube for analysis (acquisition with EDTA).

Samples were analyzed with a NMR spectrometer Advance 700 Mz (Bruker Biospin). NMR analyzes were performed at 298 K (25°C) without tube spinning, using a proton-decoupled carbon pulse program (zgig) with 90° pulses for ^{13}C (10 µs, 50 W). Acquisition parameters were: decoupling sequence waltz16, 0.9 s acquisition time, 65 k size of FID, and a relaxation delay (D1) of 1.2 s. 12,000 scans were done, representing about 9 h analysis per sample. Since the response of individual peaks at different chemical shifts is not perfectly quantitative under such acquisition conditions (short D1), signals were corrected using calibrating samples with known concentrations of standard metabolites (aspartate, malate). NMR data presented in the paper are mean±SD of n = 4 to 7 replicates.

Calculations of isotopomer distribution and labelling

Each C-atom position of malate was examined separately on the spectrum and peak areas (integrals) were obtained with TopSpin (Bruker) and converted to moles of ^{13}C m^{-2}. Values obtained with non-labelled samples (CO_2 at natural abundance) were used to compute the ^{13}C percentage at each position (denoted as p): p (in %) = $S_{total}/S_{non} \times 1.1/99 \times 100$ where S_{total} and S_{non} is the NMR signal of interest upon experiments with $^{13}CO_2$ and natural CO_2, respectively. The ^{13}C percentage (%^{13}C) was then converted to fractional labelling as l = (p/100 – 0.011)/(99 – 0.011). For each C-atom position, ^{13}C-labelling of neighbor carbon atoms was detected with the appearance of a multiplet (due to ^{13}C-^{13}C couplings) instead of a singlet. The frequency of ^{13}C-^{13}C couplings was computed using deconvolution of multiplets so as to calculate the proportion of singly (*s*), doubly (*d*), and triply (*t*) labelled molecules [see the Supporting Information in (Abadie *et al.*, 2017b) for more details on peak deconvolution]. Values were corrected for the contribution of non-labelled malate (i.e. carrying ^{13}C at natural abundance, 1.1%) to the central peak of malate multiplets. In fact, the central peak of multiplets came from both labelled (at concentration c_{lab} and 99% ^{13}C) and non-labelled atoms (at concentration c_{non} and natural abundance thus 1.1% ^{13}C). By mass-balance, the total positional signal of the multiplet observed by NMR is $S_{total} = 0.99 \cdot c_{lab} + 0.011 \cdot c_{non} = 0.99 \cdot c_{tot} - 0.979 \cdot c_{non}$, where $c_{tot} = c_{lab} + c_{non}$. The NMR signal of the central peak is $S_{centre} = 0.99 \cdot c_{lab \cdot s} + 0.011 \cdot c_{non}$ where $c_{lab \cdot s}$ is the concentration of singly ($^{13}C_1$) labelled molecules (thus $c_{lab \cdot s} < c_{lab}$). Also, by definition, in the non-labelled sample (fed with CO_2 at natural abundance), $S_{non} = 0.011 \cdot c_{tot}$. By substitution, we then obtain:

166 $$c_{lab\cdot s} = \frac{S_{centre}}{0.99} - \frac{S_{non}}{0.979} + \frac{0.011 \cdot S_{total}}{0.99 \cdot 0.979}$$

167 This calculation adds a correction to the usual calculation that neglects the 'static' pool (S_{centre}
168 – S_{non}). Nevertheless, it should be noted that this correction was small (with a S_{centre} value of
169 say, 0.6, S_{non} was about 0.1 and S_{total} about 1, meaning a correction of about 0.03 only). *s*, *d*
170 and *t* were calculated as proportions with $s = c_{lab\cdot s}/c_{lab}$, $d = c_{lab\cdot d}/c_{lab}$ and $t = c_{lab\cdot t}/c_{lab}$. Also,
171 these calculations neglect the isotope fractionation against ^{13}C by photosynthesis. In fact,
172 photosynthesis fractionates by about 20‰, meaning that during labelling, assimilated CO_2
173 was not exactly at 99% ^{13}C but slightly lower (98.98%). Nevertheless, the difference (0.02%)
174 was clearly negligible.

175 At each C-atom position, proportions *s*, *d* and *t* were modelled using probabilities of
176 multiple labelling, following the same principle as in Abadie *et al*. (2017b). For example, the
177 probability of observing the ^{13}C-1—^{13}C-2—^{12}C-3—^{12}C-4 isotopomer (#6 in Fig. 3) was
178 modelled as pr(#6) = $l_1 \times d_1 \times (1 - \text{pr}(4/1)) \times (1 - \text{pr}(3/2))$ where pr(4/1) is the probability of
179 C-4 being labelled when C-1 is labelled, and pr(3/2) is the probability of C-3 being labelled
180 when C-2 is labelled (Bayes probabilities), and subscript "1" stands for the position of interest
181 (here, C-1). pr(#*i*) (with $i \in [1,\ldots,16]$) were used to express proportions *s*, *d* and *t* and
182 fractional labelling *l*. For example, l_k (fractional labelling at C-atom position *k*) is given by:

183 $$l_k = \sum_i \text{pr}(\#i) \cdot \delta_{ik}$$

184 where $\delta_{ik} = 1$ if isotopomer *i* has a ^{13}C at C-atom position *k*, and $\delta_{ik} = 0$ otherwise. Similarly,
185 d_k (proportion of doublet labelling at position *k*) is given by:

186 $$d_k = \frac{\sum_i \text{pr}(\#i) \cdot \varphi_{ik}}{l_k}$$

187 where $\varphi_{ik} = 1$ if isotopomer *i* has a ^{13}C couple that includes position *k* (i.e. with a ^{13}C at *k*–1
188 and *k*, or *k* and *k*+1) and $\varphi_{ik} = 0$ otherwise. Bayes probabilities were then solved numerically
189 (in Excel) to match observed values of *s*, *d*, *t* and *l*. Since there were four C-atom positions,
190 there were a total of 14 observed values (C-1 and C-4 do not have triple labelling so have no *t*
191 values). To allow robust resolution, we only required six Bayes probabilities: pr(4/1), pr(4/2t)
192 (probability for C-4 being labelled when there is triple labelling at C-2), pr(1/3t) (probability
193 for C-1 being labelled when there is triple labelling at C-3), pr(3/2), pr(-1/2∩3) (probability

for C-1 not being labelled when both C-2 and C-3 are labelled), and pr(2/4). Other probabilities were computed using the law of total probability. The average error on percentages was always less than 3%, meaning that computed probability values explained very well the observed isotopic pattern.

Calculation of PEPC activity from NMR data

The ^{13}C-signal in C-4 could not be used directly to compute PEPC activity simply because of malate symmetrization by fumarase. That is, the signal in C-1 + C-4 was the average of the ^{13}C labelling due to bicarbonate and the C-1 atom of PEP. Similarly, the signal in C-2 + C-3 was the average of C-2 and C-3 atom of PEP. Thus, by mass-balance, we have:

$$S_{1/4} = (S_{3/2} + S_P)/2$$

where $S_{1/4}$ is the average of C-1 and C-4 signals, and $S_{3/2}$ is the average of C-2 and C-3 signals. S_P is the original ^{13}C-signal in malate C-4 before symmetrization. This relationship assumes that the isotope distribution in PEP is homogeneous, for which evidence has been provided previously (Abadie *et al*. 2018). Thus,

$$S_P = 2\,S_{1/4} - S_{3/2}$$

S_P can be expressed in moles ^{13}C m^{-2} and the PEPC flux of bicarbonate fixation was then calculated as $F_P = S_P/T$ where T is labelling time (7,200 s). The PEPC flux of ^{13}C represented by PEP utilisation was calculated as $F_U = 1.5 \times S_{3/2}/T$ (the coefficient 1.5 is used because PEP comprises three C-atom positions, not only two).

Results

Resolution of isotopic signals

A typical NMR spectrum of the COOH groups region is presented in Fig. 2. Without EDTA, peaks corresponding to COOH groups were not well-resolved because of coordination with bivalent cations like calcium (Ca^{2+}) and magnesium (Mg^{2+}) naturally present in the sample. As expected, the addition of EDTA significantly improved the quality of the spectrum in the carboxylate region, but added two peaks corresponding to Mg^{2+}- and Ca^{2+}-coordinated EDTA, and non-coordinated EDTA. In particular, it could be seen that the prevalent labelled COOH-containing metabolites were malate, glycerate (photorespiratory intermediate), fumarate and glycine + serine.

Malate appeared as two triplets, corresponding to C-1 and C-4 atom positions. The triplet form showed that neighbor carbon atoms (C-2 and C-3) were labelled. In fact, C-2 and C-3 NMR signals were visible and formed dissymmetric quintuplets (Fig. S2). The clear appearance of COOH groups with intensity even larger than serine and glycine shows the relatively high incorporation of ^{13}C-bicarbonate by PEPC. Also, the fact that C-1 and C-4 atom positions have nearly identical signals shows that symmetrization via fumarase (Fig. 1B) occurred. In fact, calculation of positional %^{13}C showed that C-1 and C-4 were similar and varied between 15 and 30% across the treatments, while C-2 and C-3 were similar and varied between 8 and 15% (Table S1).

The peak corresponding to aspartate was very small compared to malate. In effect, aspartate (and asparagine) appeared to be mostly labelled in the dark, showing the production of labelled oxaloacetate (at C-2) by night metabolism (Fig. S3). Citrate also appeared to be labelled during the night while it was hardly visible during the day, showing its accumulation in darkness for further utilization during the subsequent light period (Fig. S3). As expected, two amino acids did not follow this pattern, glycine and serine, due to their involvement in photorespiration. Fumarate labelling was very small during the day and without EDTA, it was even impossible to see neighbor ^{13}C of CH=CH atoms (Fig. S4). The occurrence of ^{13}C atoms in the CH=CH group was invisible using observation of the COOH signal, showing their very small labelling (Fig. 2). Taken as a whole, examination of metabolites derived from C_4 metabolism (PEPC fixation) showed that malate was by far the prevalent product under our conditions.

Isotopomer distribution

The calculated abundance of malate isotopomers (across all O_2/CO_2 conditions) is shown in Fig. 3. Amongst the 16 possible isotopomers (Fig. 3B), only 5 were abundant: First, the non-labelled species ($^{12}C_4$) at about 80% showing that malate was on average labelled at 20%. Second, the fully labelled species ($^{13}C_4$) at about 8% and then the $^{13}C_3$ isotopomers containing both ^{13}C-1 and ^{13}C-4, and the $^{13}C_2$-isotopomers containing only ^{13}C-1 and ^{13}C-4 (Fig. 3C). This clearly shows the importance of bicarbonate fixation onto C-4 and subsequent symmetrization to C-1, and that the rate of ^{13}C-bicarbonate fixation was numerically larger than ^{13}C-PEP utilization. Accordingly, Bayes probability calculation revealed that the probability of having labelling at C-4 when C-1 was labelled is extremely high (0.97) while the probability of having non-labelled C-1 while C-4 was labelled is very small (0.03) (Fig. 3D). Interestingly, the probability of having labelled C-2 (or C-3) when C-3 (C-2,

respectively) is labelled was about 0.6, showing incomplete labelling in triose phosphates that generated PEP. However, the probability for PEPC fixation for utilizing (even incompletely) labelled PEP to fix ^{13}C-bicarbonate was high (pr(2U3/4) ≈ 0.9, Fig. 3D), showing the importance of "new" (but for some of them, also containing ^{12}C due to incomplete labelling) PEP molecules to feed PEPC activity.

In vivo PEPC activity

PEPC activity calculated from isotopic incorporation is represented in Fig. 4, where O_2/CO_2 conditions are distinguished with colors. There are two ways to express PEPC activity: ^{13}C-bicarbonate consumption, or ^{13}C-PEP utilization (referred to as F_P and F_U in *Material and methods*, respectively). The two values are anticipated to be different considering the intramolecular heterogeneity of ^{13}C-labelling in malate. There was a very clear trend whereby ^{13}C-bicarbonate fixation increased as net CO_2 assimilation (and the CO_2-to-O_2 ratio) decreased. The effect of O_2/CO_2 conditions on ^{13}C-bicarbonate fixation was significant ($P < 0.01$, Table S1) so that PEPC activity was significantly higher at low assimilation (100% O_2, and 140 µmol mol^{-1} CO_2) compared to other conditions. When expressed in percentage of net assimilation, PEPC fixation was small under standard conditions and high assimilation (about 2%) but changed to 25% on average (and up to 40%) at low assimilation (Fig. 4, inset). ^{13}C-PEP utilization was much lower, ranging from 0.17 to 0.35 µmol ^{13}C m^{-2} s^{-1} (meaning 0.1 µmol PEP m^{-2} s^{-1}). While PEPC fixation of ^{13}C-bicarbonate increased significantly at low photosynthetic rates, the rate at which ^{13}C-PEP was fed to the reaction did not increase to the same extent: in fact, remobilization of non-labelled carbon to generate PEP increased, from about 70% at high photosynthetic rates to nearly 90% at low assimilation (Table S1).

Discussion

De novo malate synthesis is impacted by photosynthetic conditions

Our results provide for the first time a precise estimate of *in vivo* PEPC activity in illuminated leaves, under varying O_2/CO_2 conditions. Although our present calculations take advantage of the isotopic signal in malate only, we believe our values are representative because the redistribution of ^{13}C to products other than malate (such as aspartate) was small. Typically, in aspartate, the flux estimated with C-2 and C-3 atom positions is within the order of 0.016-0.033 µmol m^{-2} s^{-1} (Abadie *et al.*, 2017b), that is, less than 10% of the PEP flux to malate synthesis found here. It has been argued that malate synthesis could also take place in the chloroplast via the reverse reaction of NADP-dependent malic enzyme (NADP-ME; pyruvate

+ CO_2 + NADPH → malate + NADP) instead of PEPC (Bloom & Lancaster, 2018). However, this reaction is extremely unlikely for three reasons: First, the very high K_m for pyruvate (10 mM) while its chloroplastic concentration is about 5 µM only (Wheeler *et al.*, 2008; Krueger *et al.*, 2011). Second, upon $^{13}CO_2$ labelling, chloroplastic pyruvate (like PEP) is likely to be highly ^{13}C-labelled [for a similar effect in chlorogenate synthesis, see (Abadie *et al.*, 2018)] and would have produced a homogenous ^{13}C pattern in malate. Third, the reverse reaction by NADP-ME is driven by the redox power but in the illuminated chloroplast, the NADPH/NADP ratio is about 1 only in the steady-state, due to rapid NADPH consumption by the Calvin-Benson-Bassham cycle (Takahama *et al.*, 1981).

PEPC fixing activity appears to be significantly stimulated at low CO_2 or high O_2. This is consistent with previous findings that suggested an increase in the ^{13}C-build up in malate in the same species (sunflower) under similar conditions (Abadie *et al.*, 2018). This is also consistent with malate being amongst the best metabolic biomarkers of the O_2/CO_2 ratio (Fig. S1) (Abadie *et al.*, 2016a) and the stimulation of the aspartate pathway (methionine, threonine) at high oxygen (Abadie *et al.*, 2017a). However, the rationale of the effect of the carboxylation-to-oxygenation (or CO_2-to-O_2) ratio on PEPC activity is not totally clear. A reconfiguration of PEP and pyruvate metabolism has been found in Arabidopsis rosettes when O_2/CO_2 conditions are varied (Abadie *et al.*, 2016b). In effect, this study showed that there is a considerable dephosphorylation of pyruvate Pi dikinase that stimulates its activity at low CO_2, allowing PEP reformation from pyruvate, and this effect is accompanied by an increase in malate quantity. There is also a concurrent increase in pyruvate dehydrogenase activity, thereby impeding pyruvate oxidation to acetyl-CoA at low CO_2 or high O_2. Therefore, PEPC activity could be viewed as a consequence of decreased catabolism of pyruvate when photorespiration increases. It is also possible that PEPC activity is directly linked to photorespiration itself via the reductive power (generated by glycine conversion to serine) or TCAP replenishment to sustain glutamate and glutamine metabolism which is stimulated by photorespiration (the increase in the glutamine pool is visible in Fig. S1). In fact, mutants affected in malate dehydrogenase show an alteration in photorespiratory metabolism (Cousins *et al.*, 2008; Tomaz *et al.*, 2010). In addition, mutants affected in glutamine-2-oxoglutarate amino transferase do exhibit an increase in PEPC activity that correlates to leaf glutamine content (Ferrario-Mery *et al.*, 2002). Finally, an increased PEPC activity might be viewed as beneficial for carbon balance by increasing photorespiratory CO_2 refixation. We note however that malate is substantially decarboxylated in the first minutes of darkness (LEDR) therefore the net carbon gain provided by refixation into malate is probably modest.

The mechanism by which PEPC activity is modulated by O_2/CO_2 conditions is likely to be a balance between changes in substrate availability, allosteric effects and post-translational modifications (O'Leary & Plaxton, 2017). We hypothesize that at high photosynthetic rates, PEPC was slightly less phosphorylated but could be stimulated by higher cytosolic concentration in fructose 6-phosphate. At low photosynthetic rates, it was slightly more phosphorylated, PEP was more available but it could be inhibited by its product, malate. The net result of these influences was a clear stimulation at low photosynthetic rates. However, it likely depends on physiological conditions such as nitrogen metabolism, and not only O_2/CO_2. Typically, nitrate availability affects leaf PEPC activity (Sharma & Sirohi, 1988). In addition, PEP can be used by secondary metabolism. In sunflower, chlorogenate synthesis is negatively impacted by photorespiration (Abadie *et al.*, 2018) and this should in principle increase PEP availability, but chlorogenate metabolism also depends on nutrient conditions and age (Koeppe *et al.*, 1970; Lehman & Rice, 1972).

Consequences for photosynthetic gas-exchange

Our findings may have quantitatively important consequences for photosynthetic gas-exchange. In fact, observed net assimilation is usually believed to reflect mostly the net flux of carboxylation, photorespiratory CO_2 release, and day respiration. PEPC fixation is often assumed to be small and possibly embedded into day respiration, at a constant rate. Although PEPC utilizes bicarbonate and not CO_2, this matters because under the assumption that the cellular bicarbonate pool is in the steady-state, the consumption of HCO_3^- has to be compensated for by gaseous CO_2 consumption by the leaf. In fact, cellular bicarbonate concentration has to be constant because under controlled gas-exchange conditions whereby internal CO_2 mole fraction, c_c, is in the steady-state, bicarbonate remains constant while cellular pH remains constant. Hence, our finding that PEPC fixation varies with O_2/CO_2 conditions and represents a large flux at low photosynthetic rates is highly significant. It should also be noted that even at high photosynthetic rates, it represents about 0.3 µmol m^{-2} s^{-1}, which is not negligible as compared to commonly measured day respiratory rates (≈0.5 µmol m^{-2} s^{-1}). Usually, net photosynthesis is modelled as (Farquhar *et al.*, 1980; Von Caemmerer & Farquhar, 1981):

$$A = v_c \cdot \left(1 - \frac{\Gamma^*}{c_c}\right) - R_d$$

where Γ^* is the CO_2 compensation point in the absence of day respiration, v_c is Rubisco-catalyzed carboxylation velocity (and can be modelled by Rubisco Michaelis kinetics) and R_d is day respiration. If PEPC fixation (denoted as P) is not encapsulated by R_d, then the equation can be re-written as:

$$A = v_c \cdot \left(1 - \frac{\Gamma^*}{c_c}\right) - R_d + P$$

To give a numerical estimate of the impact of P on photosynthesis, we performed here very simple calculations of v_c using *(i)* observed values of A and P, assuming that R_d = 0.5 µmol m^{-2} s^{-1} and *(ii)* c_i-based Γ^* (43 µmol mol^{-1}) and c_i instead of c_c simply because internal conductance was not determined in the present study. Results are shown in Fig. 5. As expected, the impact of P on calculated v_c is extremely small at ordinary CO_2 and O_2 mole fractions. However, at high O_2 (100%) or low CO_2 (140 µmol mol^{-1}), v_c is systematically over-estimated when P is not considered. The principle of these calculations might change if there is a concurrent modification of internal conductance (g_m) with O_2/CO_2 conditions. Similar labelling and metabolomics experiments in sunflower whereby g_m was estimated using the $^{16}O/^{18}O$ isotope discrimination suggested that there were minimal changes in internal conductance, except at 800 µmol mol^{-1} CO_2 and 100% O_2 where it decreased approximately two-fold (Abadie *et al.*, 2017a). Under such conditions, actual c_c and thus v_c should be lower (compared with a calculation that would assume constant internal conductance) and thus the error made by neglecting P would be even larger.

The impact of P is thus relatively important at low photosynthetic rates, and this may be problematic when carrying out, e.g., Laisk curves to measure Γ^*_i and R_d, because this type of experiment is done at low CO_2. That is, it probably leads to a misestimation of the compensation point. In fact, a relationship has been found between PEPC activity in leaf extracts and observed CO_2 compensation point in wheat (Sharma & Sirohi, 1988). By contrast, P varies with CO_2 mole fraction (present work) and thus participates in the variation of apparent assimilation and as such, should not compromise R_d estimation [provided R_d remains constant regardless of CO_2 mole fraction, an assumption that might be incorrect (Tcherkez *et al.*, 2017)]. It is worth noting that at first glance, our results may appear opposite to those obtained in transgenic lines with an increased PEPC activity, which do not show an increased (but slightly decreased) photosynthetic rate (Hudspeth *et al.*, 1992; Gehlen *et al.*, 1996). Nevertheless, it should be remembered that PEPC overexpression is associated with strong pleiotropic effects such as intracellular inorganic phosphate (P_i) deficiency that inhibits

photosynthetic metabolism (Agarie *et al.*, 2002) and a considerable increase in day respiration rate (R_d), thereby compensating for increased PEPC fixation in the light [for a review, see (Miyao & Fukayama, 2003)].

Also, using modelling, it has been suggested that changes in nitrogen assimilation at low photosynthetic rates caused by photorespiration-driven build-up of serine and glycine can modify the response of net assimilation to CO_2 mole fraction (Busch *et al.*, 2018). Our results further suggest that PEPC activity could also contribute to shaping the photosynthesis response curve to CO_2 since it represents roughly 1 µmol m^{-2} s^{-1} at low photosynthetic rates (Fig. 4) and thus an electron sink of about 2 µmol m^{-2} s^{-1} (electrons are required to reduce oxaloacetate to malate).

Perspectives

The present study shows that PEPC activity in C_3 leaves cannot be neglected in the CO_2 budget of gas exchange, particularly at low photosynthetic rates under low CO_2 or high O_2. However, the overall impact of PEPC activity on the carbon plant budget deserves further work. In the natural environment, low CO_2 conditions (low c_i) occur during, e.g., drought, and thus are associated with other stresses that may also affect the photosynthetic machinery. Still, our NMR technology offers a precise method to measure *in vivo* PEPC activity. This could now be exploited further to investigate the effect of environmental conditions such as N availability, or to examine other C_3 species that have different PEPC enzymatic capacity and accumulate different organic acids. In fact, sunflower contains extremely small amount of citrate but has significant amounts of malate and fumarate. Other species like rapeseed (*Brassica napus*) contain citrate and have a very small amount of fumarate, suggesting that PEPC activity in the light might be lower. Nutrient availability (N, P and K) is also likely to reorchestrate respiratory metabolism (Rivas-Ubach *et al.*, 2012) and change PEPC activity accordingly, but this has never been examined quantitatively [for a review, see (Tcherkez, 2017)]. The effect of light would also be of great interest, particularly at low light (i.e., near or below the compensation point) where there is an increase in the quantum yield of photosynthesis (Kok effect). However, alternative, more sensitive technologies would have to be developed because photosynthetic rates are very low or negative in these conditions and so ^{13}C-NMR may not be adapted to quantify PEPC activity. This will be addressed in a subsequent study.

Acknowledgements

The authors thank the *Australian Research Council* for its financial support through a *Future Fellowship*, under contract FT140100645. The authors also thank Benjamin Siegler (Moltech Anjou, University of Angers, France) for preliminary NMR analyses.

Author contributions

CA performed experiments. CA and GT undertook NMR analyses. GT wrote the paper.

References

Abadie C, Bathellier C, Tcherkez G. 2018. Carbon allocation to major metabolites in illuminated leaves is not just proportional to photosynthesis when gaseous conditions (CO_2 and O_2) vary. *New Phytologist* **218**: 94-106.

Abadie C, Blanchet S, Carroll A, Tcherkez G. 2017a. Metabolomics analysis of postphotosynthetic effects of gaseous O_2 on primary metabolism in illuminated leaves. *Functional Plant Biology* **44**: 929-940.

Abadie C, Boex-Fontvieille ER, Carroll AJ, Tcherkez G. 2016a. *In vivo* stoichiometry of photorespiratory metabolism. *Nature plants* **2**: 15220.

Abadie C, Lothier J, Boex-Fontvieille E, Carroll A, Tcherkez G. 2017b. Direct assessment of the metabolic origin of carbon atoms in glutamate from illuminated leaves using ^{13}C-NMR. *New Phytologist* **216**: 1079-1089.

Abadie C, Mainguet S, Davanture M, Hodges M, Zivy M, Tcherkez G. 2016b. Concerted changes in the phosphoproteome and metabolome under different CO_2/O_2 gaseous conditions in Arabidopsis rosettes. *Plant and Cell Physiology* **57**: 1544-1556.

Agarie S, Miura A, Sumikura R, Tsukamoto S, Nose A, Arima S, Matsuoka M, Miyao-Tokutomi M. 2002. Overexpression of C_4 PEPC caused O_2-insensitive photosynthesis in transgenic rice plants. *Plant Science* **162**: 257-265.

Amory AM, Vanlerberghe GC, Turpin DH. 1991. Demonstration of both a photosynthetic and a nonphotosynthetic CO_2 requirement for NH_4^+ assimilation in the green alga *Selenastrum minutum*. *Plant Physiology* **95**: 192-196.

Bloom AJ, Lancaster KM. 2018. Manganese binding to Rubisco could drive a photorespiratory pathway that increases the energy efficiency of photosynthesis. *Nature plants* **4**: 414-422.

Busch FA, Sage RF, Farquhar GD. 2018. Plants increase CO_2 uptake by assimilating nitrogen via the photorespiratory pathway. *Nature plants* **4**: 46.

Chollet R, Vidal J, O'Leary MH. 1996. Phospho*enol*pyruvate carboxylase: a ubiquitous, highly regulated enzyme in plants. *Annual Review of Plant Physiology and Plant Molecular Biology* **47**: 273-298.

Cousins AB, Pracharoenwattana I, Zhou W, Smith SM, Badger MR. 2008. Peroxisomal malate dehydrogenase is not essential for photorespiration in *Arabidopsis* but its absence causes an increase in the stoichiometry of photorespiratory CO_2 release. *Plant Physiology* **148**: 786-795.

Farquhar GD, von Caemmerer S, Berry J. 1980. A biochemical model of photosynthetic CO_2 assimilation in leaves of C_3 species. *Planta* **149**: 78-90.

Ferrario-Mery S, Hodges M, Hirel B, Foyer CH. 2002. Photorespiration-dependent increases in phospho*enol*pyruvate carboxylase, isocitrate dehydrogenase and glutamate dehydrogenase in transformed tobacco plants deficient in ferredoxin-dependent glutamine–α-ketoglutarate aminotransferase. *Planta* **214**: 877-886.

Fukayama H, Fujiwara N, Hatanaka T, Misoo S, Miyao M. 2014. Nocturnal phosphorylation of phospho*enol*pyruvate carboxylase in the leaves of hygrophytic C_3 monocots. *Bioscience, Biotechnology, and Biochemistry* **78**: 609-613.

Fukayama H, Tamai T, Taniguchi Y, Sullivan S, Miyao M, Nimmo HG. 2006. Characterization and functional analysis of phospho*enol*pyruvate carboxylase kinase genes in rice. *The Plant Journal* **47**: 258-268.

Gauthier PG, Bligny R, Gout E, Mahé A, Nogués S, Hodges M, Tcherkez Guillaume GB. 2010. *In folio* isotopic tracing demonstrates that nitrogen assimilation into glutamate is mostly independent from current CO_2 assimilation in illuminated leaves of *Brassica napus*. *New Phytologist* **185**: 988-999.

Gehlen J, Panstruga R, Smets H, Merkelbach S, Kleines M, Porsch P, Fladung M, Becker I, Rademacher T, Häusler RE, et al. 1996. Effects of altered phospho*enol*pyruvate carboxylase activities on transgenic C_3 plant *Solanum tuberosum*. *Plant molecular biology* **32**: 831-848.

Gessler A, Tcherkez G, Karyanto O, Keitel C, Ferrio JP, Ghashghaie J, Kreuzwieser J, Farquhar GD. 2009. On the metabolic origin of the carbon isotope composition of

CO_2 evolved from darkened light-acclimated leaves in *Ricinus communis*. *New Phytologist* **181**: 374-386.

Hudspeth RL, Grula JW, Dai Z, Edwards GE, Ku MS. 1992. Expression of maize phospho*enol*pyruvate carboxylase in transgenic tobacco: effects on biochemistry and physiology. *Plant Physiology* **98**: 458-464.

Koeppe DE, Rohrbaugh LM, Rice EL, Wender SH. 1970. Tissue age and caffeoylquinic acid concentration in sunflower. *Phytochemistry* **9**: 297-301.

Krömer S, Gardeström P, Samuelsson G. 1996a. Regulation of the supply of cytosolic oxaloacetate for mitochondrial metabolism via phospho*enol*pyruvate carboxylase in barley leaf protoplasts I. The effect of covalent modification on PEPC activity, pH response, and kinetic properties. *Biochimica et Biophysica Acta (BBA) - General Subjects* **1289**: 343-350.

Krömer S, Gardeström P, Samuelsson G. 1996b. Regulation of the supply of oxaloacetate for mitochondrial metabolism via phospho*enol*pyruvate carboxylase in barley leaf protoplasts II. Effects of metabolites on PEPC activity at different activation states of the protein. *Biochimica et Biophysica Acta (BBA) - General Subjects* **1289**: 351-361.

Krueger S, Giavalisco P, Krall L, Steinhauser M-C, Büssis D, Usadel B, Flügge U-I, Fernie AR, Willmitzer L, Steinhauser D. 2011. A topological map of the compartmentalized *Arabidopsis thaliana* leaf metabolome. *PLoS One* **6**: e17806.

Lehman RH, Rice EL. 1972. Effect of deficiencies of nitrogen, potassium and sulfur on chlorogenic acids and scopolin in sunflower. *The American Midland Naturalist* **87**: 71-80.

Marlier JF, O'Leary MH. 1984. Carbon kinetic isotope effects on the hydration of carbon dioxide and the dehydration of bicarbonate ion. *Journal of the American Chemical Society* **106**: 5054-5057.

Masumoto C, Miyazawa S-I, Ohkawa H, Fukuda T, Taniguchi Y, Murayama S, Kusano M, Saito K, Fukayama H, Miyao M. 2010. Phospho*enol*pyruvate carboxylase intrinsically located in the chloroplast of rice plays a crucial role in ammonium assimilation. *Proceedings of the National Academy of Sciences* **107**: 5226-5231.

Meimoun P, Gousset-Dupont A, Lebouteiller B, Ambard-Bretteville F, Besin E, Lelarge C, Mauve C, Hodges M, Vidal J. 2009. The impact of PEPC phosphorylation on growth and development of *Arabidopsis thaliana*: Molecular and physiological characterization of PEPC kinase mutants. *FEBS Letters* **583**: 1649-1652.

Miyao M, Fukayama H. 2003. Metabolic consequences of overproduction of phospho*enol*pyruvate carboxylase in C_3 plants. *Archives of Biochemistry and Biophysics* **414**: 197-203.

O'Leary BM, Plaxton WC 2017. Mechanisms and functions of post-translational enzyme modifications in the organization and control of plant respiratory metabolism. In: Tcherkez G, Ghashghaie J eds. *Plant respiration: metabolic fluxes and carbon balance*. Cham: Springer, 261-284.

O'Leary MH, Rife JE, Slater JD. 1981. Kinetic and isotope effect studies of maize phospho*enol*pyruvate carboxylase. *Biochemistry* **20**: 7308-7314.

Oja V, Savchenko G, Jakob B, Heber U. 1999. pH and buffer capacities of apoplastic and cytoplasmic cell compartments in leaves. *Planta* **209**: 239-249.

Raven JA, Farquhar GD. 1990. The influence of N metabolism and organic acid synthesis on the natural abundance of isotopes of carbon in plants. *New Phytologist* **116**: 505-529.

Rivas-Ubach A, Sardans J, Pérez-Trujillo M, Estiarte M, Peñuelas J. 2012. Strong relationship between elemental stoichiometry and metabolome in plants. *Proceedings of the National Academy of Sciences USA* **109**: 4181-4186.

Roeske C, O'Leary MH. 1984. Carbon isotope effects on enzyme-catalyzed carboxylation of ribulose bisphosphate. *Biochemistry* **23**: 6275-6284.

Sharma SN, Sirohi GS. 1988. The effect of ammonium and nitrate on carbondioxide compensation point and enzymes associated with carbondioxide exchange in wheat. *Photosynthesis Research* **17**: 267-275.

Takahama U, Shimizu-Takahama M, Heber U. 1981. The redox state of the NADP system in illuminated chloroplasts. *Biochimica et Biophysica Acta (BBA)-Bioenergetics* **637**: 530-539.

Tcherkez G 2017. Traking the orchestration of the tricarboxylic acid pathway in plants, 80 years after the discovery of the Krebs cycle. In: Tcherkez G, Ghashghaie J eds. *Plant respiration: metabolic fluxes and carbon balance*. Cham: Springer, 285-298.

Tcherkez G, Gauthier P, Buckley TN, Busch FA, Barbour MM, Bruhn D, Heskel MA, Gong XY, Crous KY, Griffin K. 2017. Leaf day respiration: low CO_2 flux but high significance for metabolism and carbon balance. *New Phytologist* **216**: 986-1001.

Tcherkez G, Mahé A, Gauthier P, Mauve C, Gout E, Bligny R, Cornic G, Hodges M. 2009. *In folio* respiratory fluxomics revealed by ^{13}C isotopic labeling and H/D isotope

effects highlight the noncyclic nature of the tricarboxylic acid “cycle” in illuminated leaves. *Plant Physiology* **151**: 620-630.

Tomaz T, Bagard M, Pracharoenwattana I, Lindén P, Lee CP, Carroll AJ, Ströher E, Smith SM, Gardeström P, Millar AH. 2010. Mitochondrial malate dehydrogenase lowers leaf respiration and supports photorespiratory carbon flux and plant growth in *Arabidopsis*. *Plant Physiology* **154**: 1143-1157.

Turpin DH, Vanlerberghe GC, Amory AM, Guy RD. 1991. The inorganic carbon requirements for nitrogen assimilation. *Canadian Journal of Botany* **69**: 1139-1145.

von Caemmerer S. 2013. Steady-state models of photosynthesis. *Plant, Cell & Environment* **36**: 1617-1630.

Von Caemmerer S, Farquhar GD. 1981. Some relationships between the biochemistry of photosynthesis and the gas exchange of leaves. *Planta* **153**: 376-387.

Wheeler MCG, Arias CL, Tronconi MA, Maurino VG, Andreo CS, Drincovich MF. 2008. *Arabidopsis thaliana* NADP-malic enzyme isoforms: high degree of identity but clearly distinct properties. *Plant molecular biology* **67**: 231-242.

Supporting Information

Table S1: additional numerical data for PEPC activity

Fig. S1: Metabolome kinetics and malate content

Fig. S2: ^{13}C-NMR signal of malate C-2 and C-3

Fig. S3: NMR spectrum of the 40-57 ppm region

Fig. S4: NMR magnification of the CH=CH signal in fumarate

Fig. 1 Simplified malate metabolism. (a) Malate synthesis via the phosph*enol*pyruvate carboxylase (PEPC)-pathway (highlighted in blue) from phospho*enol*pyruvate (PEP) and bicarbonate, which equilibrates with dissolved CO_2. Metabolite exchange between compartments is shown in pink. The figure shows fumarate as the largest non-sugar metabolite pool in sunflower leaves. (b) Origin of C-atoms in malate and mechanism of symmetrization by fumarase. Carbon numbering in malate follows the international IUPAC nomenclature. OAA, oxaloacetate; TCAP, tricarboxylic acid pathway. For simplicity, photorespiration and OAA-malate redox shuttles between compartments are not shown in this figure.

Fig. 2 Typical ^{13}C-NMR spectrum of the 172–182 ppm region, showing peaks of malate C-1 and C-4: leaf extract after $^{13}CO_2$ labelling (under 21% O_2, 380 µmol mol^{-1} CO_2) analysed with (blue) or without (red) EDTA. An authentic malate standard in water (without EDTA) is also shown for comparison (green). Note the [^{13}C-^{13}C] couplings (triplets) in sample (blue), showing isotopic labelling in neighbor C atoms (C-2 and C-3). Maleate is the internal standard. Note that fumarate does not appear as a triplet, demonstrating its very small ^{13}C-labelling. Glycine and serine have very close chemical shifts, so that their combined signals form a triplet of doublets. Also note that aspartate labelling is extremely small as compared to malate.

Fig. 3 Isotopomer distribution of labelled malate measured by NMR. (a) C-atom numbering in malate. (b) List of isotopomers species with corresponding numbers. (c) Frequency of isotopomer species (numbers listed in b). (d) Bayesian probability of multiple labelling: pr(4/1), probability of C-4 atom position being labelled when C-1 is labelled; pr(-1/4), probability of C1 not being labelled when C-4 is labelled; pr(2U3/4), probability of C-2 or C-3 being labelled when C-4 is labelled; pr(2/3), probability of C-2 being labelled when C-3 is labelled; and pr(3/2), probability of C-3 being labelled when C-2 is labelled. Values shown in (c) and (d) are mean ± SE across all gaseous conditions.

Fig. 4 Phosph*enol*pyruvate carboxylase (PEPC) flux as a function of net photosynthetic assimilation (*A*), expressed in µmol ^{13}C m^{-2} s^{-1} in a $^{13}CO_2$ atmosphere, under different gaseous conditions (given as O_2 in %, CO_2 in µmol mol^{-1}): the flux is expressed in either bicarbonate (HCO_3^-) fixation (circles) or PEP utilization (squares). Dotted lines are exponential decay regression lines (bicarbonate, R = 0.74; PEP, R = 0.40). Inset, bicarbonate fixation expressed in % of net assimilation. The red dashed line stands for PEPC activity = 0.02·*A*. The PEPC flux is calculated from direct isotopic measurements in malate by NMR (see the Materials and Methods section).

Fig. 5 Relationship between carboxylation velocity (V_c) calculated with (*y*-axis) and without (*x*-axis) the phosph*enol*pyruvate carboxylase (PEPC) correction. The continuous line stands for a linear regression (R^2 = 0.983, P < 0.001). The dotted red line is the 1 : 1 line. Colors corresponding to gas-exchange (O_2/CO_2) conditions are the same as in Fig. 4.

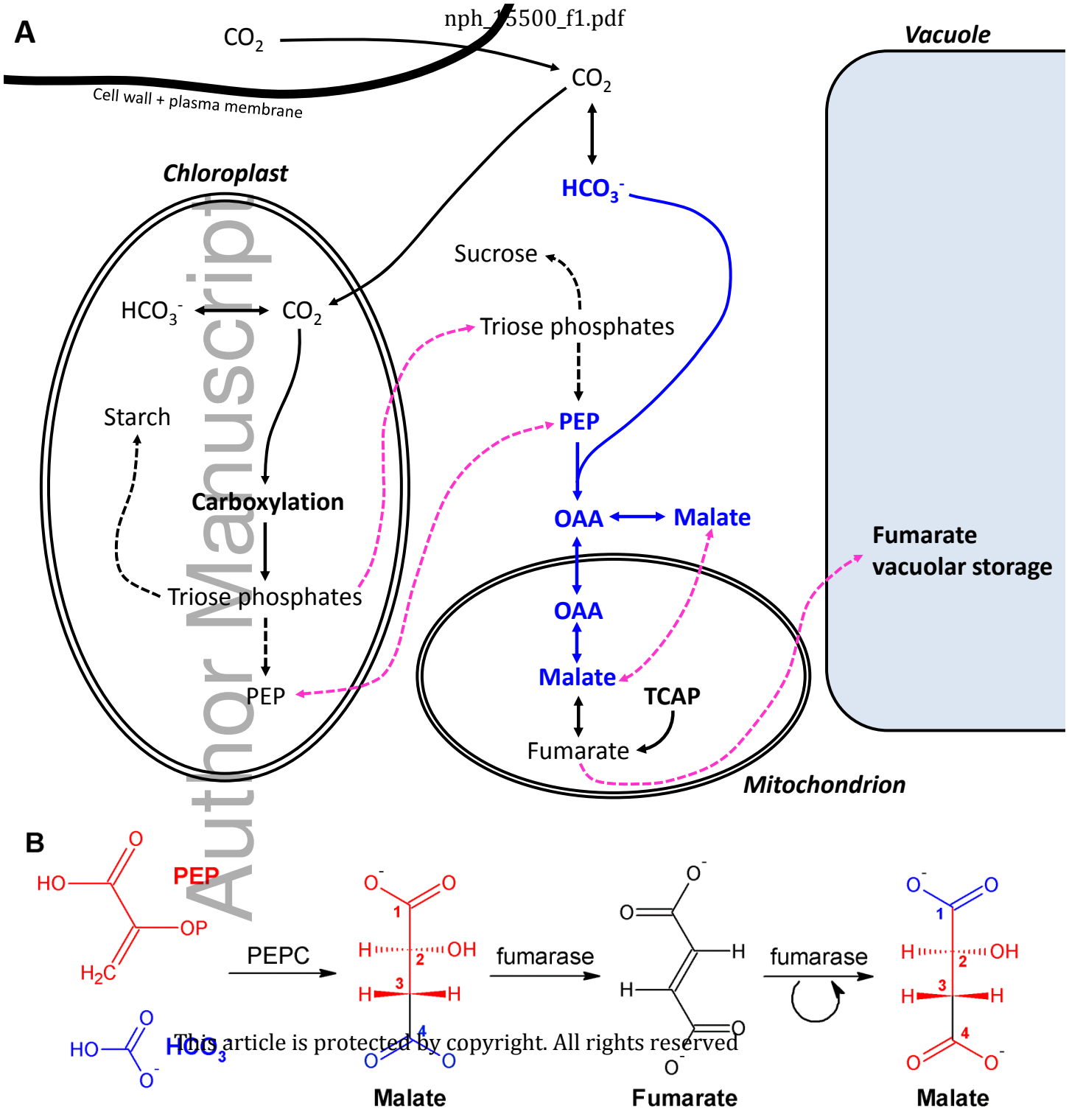

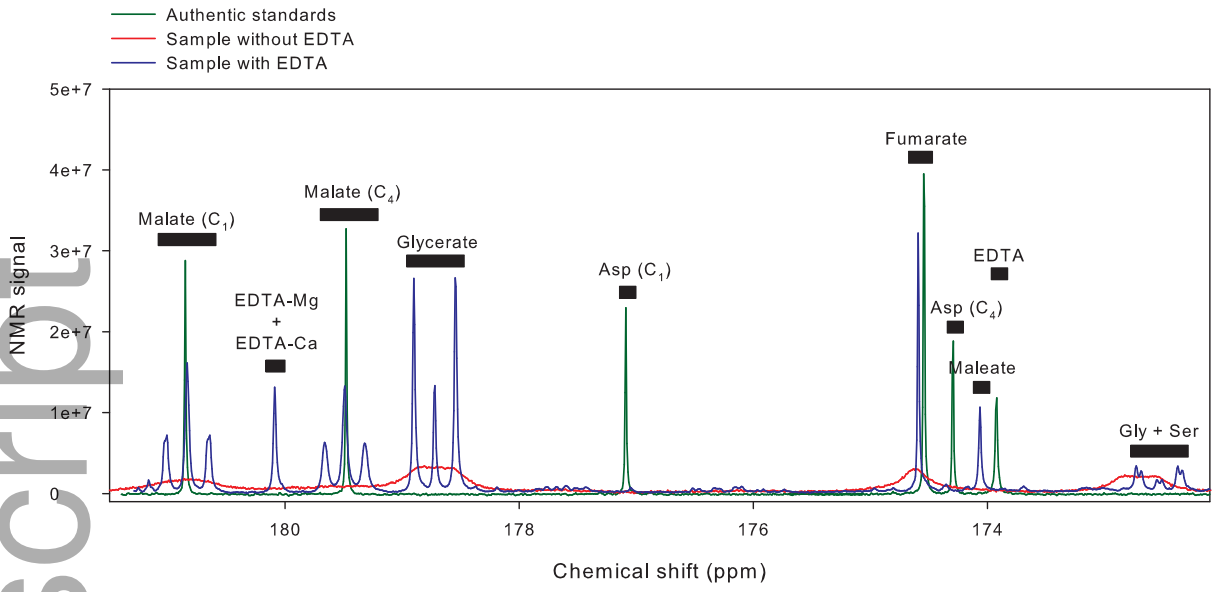

nph_15500_f2.eps

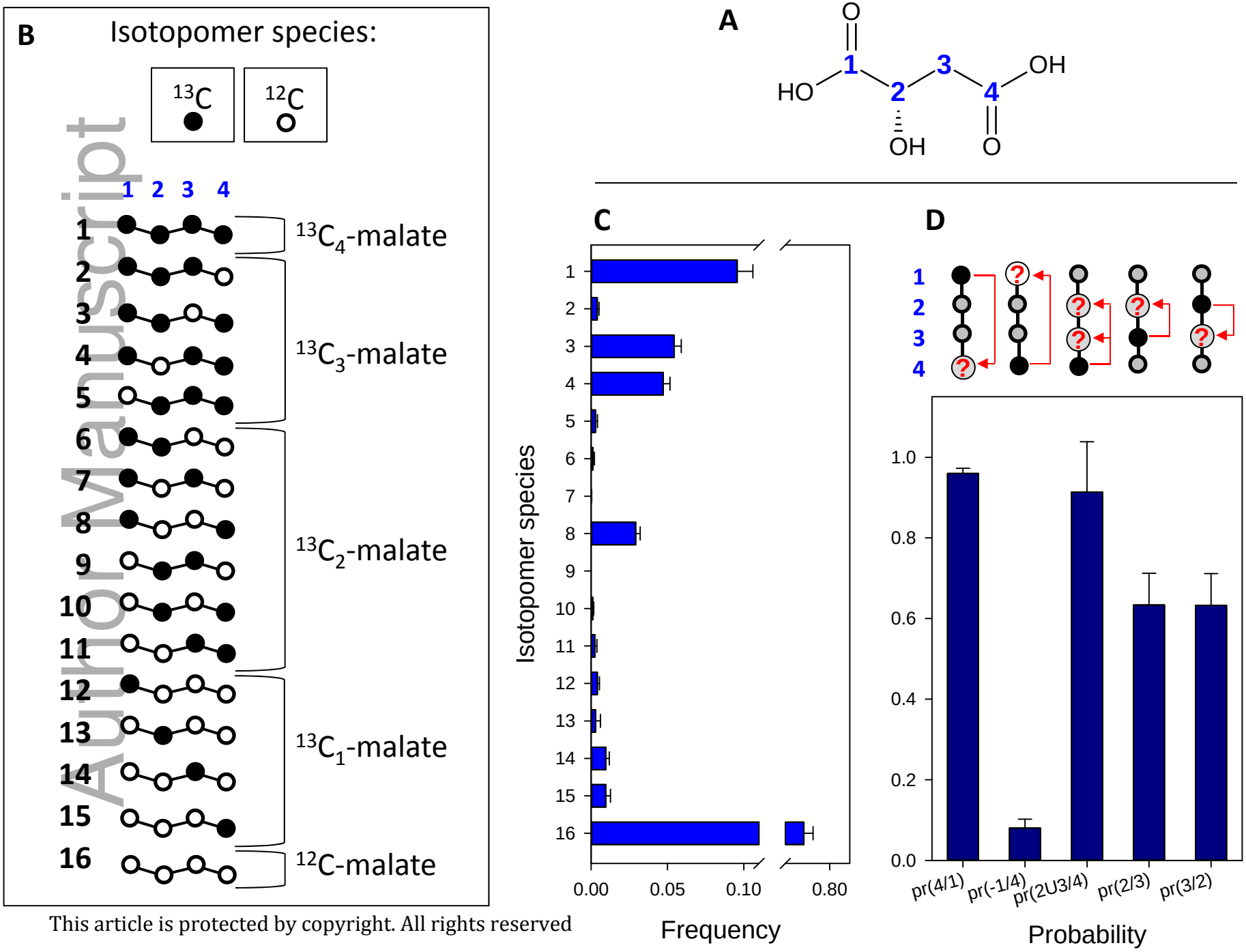

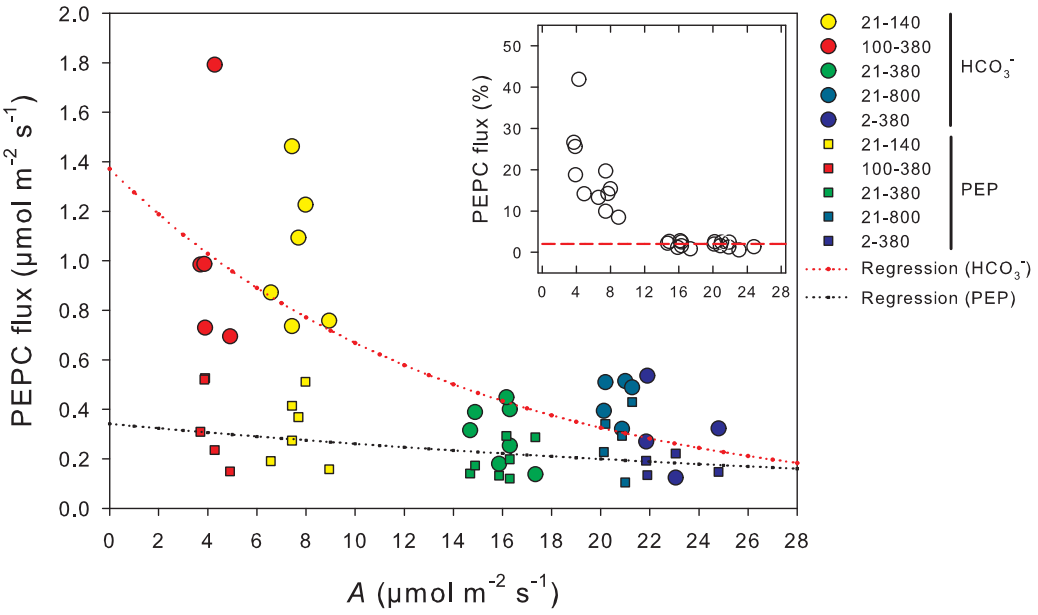

nph_15500_f4.eps

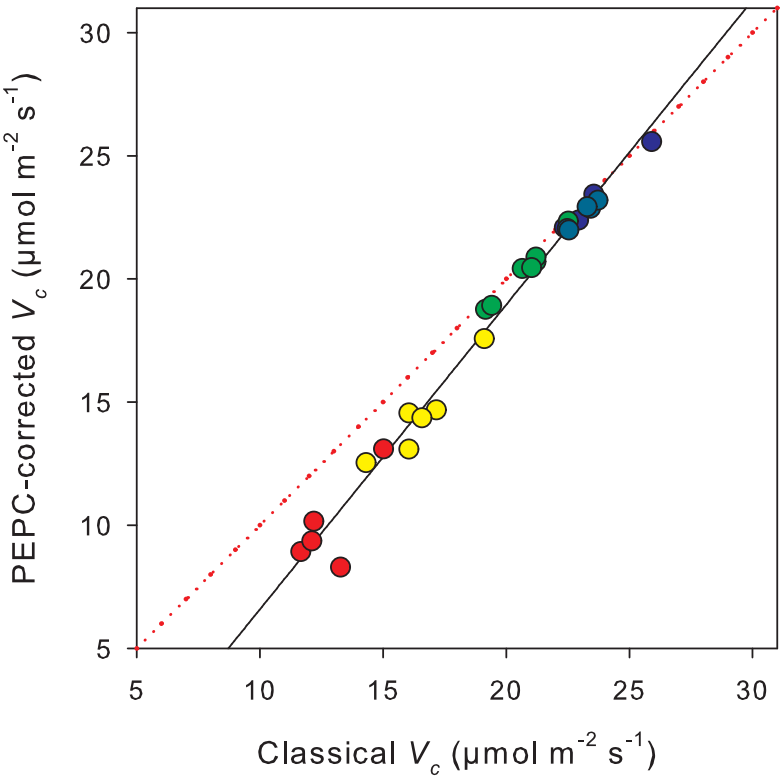

nph_15500_f5.eps